Electric charge controls plasmodesma conductivity

Alexander H. Howell, Anneline H. Christensen, Vincent James, Viktoriya V. Vasina, Kaare H. Jensen, James Foley, James E. Evans, Howard A. Stone, Winfried S. Peters & Michael Knoblauch

SUPPLEMENTARY TABLES & FIGURES

Supplementary Table 1. Small fluorescent tracers previously employed to visualize plasmodesmal permeability. Molecular masses and electric charges of the dominant molecule form at pH 7.0 are based on currently available information and do not necessarily equal the values given in the original papers. The references represent an incomplete selection.

Fluorophore	Mass (Da)	Net Charge (at pH 7)	Reference(s)
Fluorescein (Uranin)	332	−2	2, 10, 12, 14, 23, 25
Carboxyfluorescein	376	−3	3, 4, 5, 6, 11, 13, 19, 20, 21, 24, 26, 28
Lucifer Yellow CH	443	−2	2, 3, 4, 5, 8, 10, 15, 16, 18, 22, 23, 27
HPTS	455	−3	28
Cascade Blue hydrazide	527	−3	17
Sulforhodamine G	530	−2	2
Alexa Fluor 488	546	−2	7
Sulforhodamine B (Lissamine Rhodamine B)	559	−1	1, 23
Sulforhodamine 101	607	−1	18
Texas Red sulfonyl chloride	625	0	9
Alexa Fluor 568	708	−2	7
Alexa 568 hydrazide	731	?	1
Alexa Fluor 633	1150	−2	7

1. Barton, D.A., Cole, L., Collings, D.A., Liu, D.Y.T., Smith, P.M.C., Day, D.A. & Overall, R.L. Cell-to-cell transport via the lumen of the endoplasmic reticulum. *Plant J.* **66**, 806–817 (2011).
2. Christensen, N.M., Faulkner, C. & Oparka, K. Evidence for unidirectional flow through plasmodesmata. *Plant Physiol.* **150**, 96–104 (2009).
3. Derrick, P.M., Barker, H. & Oparka, K.J. Effect of virus infection on symplastic transport of fluorescent tracers in *Nicotiana clevelandii* leaf epidermis. *Planta* **181**, 555–559 (1990).

4. Duckett, C.M., Oparka, K.J., Prior, D.A.M., Dolan, L. & Roberts, K. Dye-coupling in the root epidermis of *Arabidopsis* is progressively reduced during development. *Development* **120**, 3247–3255 (1994).

5. Goodwin, P.B., Shepherd, V. & Erwee, M.G. Compartmentation of fluorescent tracers injected into the epidermal cells of *Egeria densa* leaves. *Planta* **181**, 129–136 (1990).

6. Gui, J., Liu, C., Shen, J. & Li, L. *Grain setting defect1*, encoding a remorin protein, affects the grain setting in rice through regulating plasmodesmatal conductance. *Plant Physiol.* **166**, 1463–1478 (2014).

7. Howell, A.H., Peters, W.S. & Knoblauch, M. The diffusive injection micropipette (DIMP). *J. Plant Physiol.* **21**, 153060 (2020).

8. Ishiwatari, Y., Fujiwara, T., McFarland, K.C., Nemoto, K., Hayashi, H., Chino, M. & Lucas, W.J. Rice phloem thioredoxin h has the capacity to mediate its own cell-to-cell transport through plasmodesmata. *Planta* **205**, 12–22 (1998).

9. Kempers, R., Prior, D.A.M., Oparka, K.J., Knoblauch, M. & van Bel, A.J.E. Integration of controlled intracellular pressure microinjection, iontophoresis, and membrane potential measurement. *Plant Biol.* **1**, 31–37 (1999).

10. Kragler, F. Analysis of the conductivity of plasmodesmata by microinjection. In: *Plasmodesmata: methods and protocols*, Methods in Molecular Biology 1217 (ed.: M. Heinlein). New York: Springer (2015).

11. Lee, J.-Y., Wang, X., Cui, W., Sager, R., Modla, S., Czymmek, K., Zybaliov, B., van Wijk, K., Zhang, C., Lu, H. & Lakshmanan, V. A plasmodesmata-localized protein mediates crosstalk between cell-to-cell communication and innate immunity in *Arabidopsis*. *Plant Cell* **23**, 3353–3373 (2011).

12. Liesche, J. & Schulz, A. In vivo quantification of cell coupling in plants with different phloem-loading strategies. *Plant Physiol.* **159**, 355–365 (2012).

13. Liu, N.-J., Zhang, T., Liu, Z.-H., Chen, X., Guo, H.-S., Ju, B.-H., Zhang, Y.-Y., Li, G.-Z., Zhou, Q.-H., Qin, Y.-M. & Zhu, Y.-X. Phytosphinganine affects plasmodesmata permeability via facilitating PDLP5-stimulated callose accumulation in *Arabidopsis*. *Mol. Plant* **13**, 128–143 (2020).

14. Mogensen, H.L. Translocation of uranin within the living ovules of selected species. *Amer. J. Bot.* **68**, 195–199 (1981).

15. Oparka, K.J., Murphy, R., Derrick, P.M., Prior, D.A.M. & Smith, J.A.C. Modification of the pressure-probe technique permits controlled intracellular microinjection of fluorescent probes. *J. Cell Sci.* **98**, 539–544 (1991).

16. Oparka, K. & Prior, D.A.M. Movement of Lucifer Yellow CH in potato tuber storage tissues: a comparison of symplastic and apoplastic transport. *Planta* **176**, 533–540 (1988).

17. Poirson, A., Turner, A.P., Giovane, C., Berna, A., Roberts, K. & Godefroy-Colburn, T. Effects of the alfalfa mosaic virus movement protein expressed in transgenic plants on the permeability of plasmodesmata. *J. Gen. Virol.* **74**, 2456–2461 (1993).

18. Radford, J.E. & White, R.G. Effects of tissue-preparation-induced callose synthesis on estimates of plasmodesma size exclusion limits. *Protoplasma* **216**, 47–55 (2001).

19. Ross-Elliott, T.J., Jensen, K.H., Haaning, K.S., Wager, B.M., Knoblauch, J., Howell, A.H., Mullendore, D.L., Monteith, A.G., Pailtre, D., Yan, D., Otero, S., Bourdon, M., Sager, R., Lee, J.-Y., Helariutta, Y., Knoblauch, M. & Oparka, K.J. Phloem unloading in *Arabidopsis* roots is convective and regulated by the phloem-pole pericycle. *eLife* **6**, e24125 (2017).

20. Ruan, Y.-L., Llewellyn, D.J. & Furbank, R.T. The control of single-celled cotton fiber elongation by developmentally reversible gating of plasmodesmata and coordinated expression of sucrose and K^+ transporters and expansin. *Plant Cell* **13**, 47–60 (2001).

21. Rutschow, H.L., Baskin, T.I. & Kramer, E.M. Regulation of solute flux through plasmodesmata in the root meristem. *Plant Physiol.* **155**, 1817–1826 (2011).

22. Su, S., Liu, Z., Chen, C., Zhang, Y., Wang, X., Zhu, L., Miao, L., Wang, X.-C. & Yuan, M. *Cucumber Mosaic Virus* movement protein severs actin filaments to increase the plasmodesmal size exclusion limit in tobacco. *Plant Cell* **22**, 1373–1387 (2010).

23. Terry, B.R. & Robards, A.W. Hydrodynamic radius alone governs the mobility of molecules through plasmodesmata. *Planta* **171**, 145–157 (1987).

24. Tucker, J.E., Mauzerall, D. & Tucker, E.B. Symplastic transport of carboxyfluorescein in staminal hairs of *Setcreasea purpurea* is diffusive and includes loss to the vacuole. *Plant Physiol.* **90**, 1143–1147 (1989).

25. Tyree, M.T. & Tammes, P.M.L. Translocation of uranin in the symplasm of staminal hairs of *Tradescantia*. *Can. J. Bot.* **53**, 2038–2046 (1975).

26. Wang, N. & Fisher, D.B. The use of fluorescent tracers to characterize the post-phloem transport pathway in maternal tissues of developing wheat grains. *Plant Physiol.* **104**, 17–27 (1994).

27. Wolf, S., Deom, C.M., Beachy, R.N. & Lucas, W.J. Movement protein of tobacco mosaic virus modifies plasmodesmatal size exclusion limit. *Science* **246**, 377–379 (1989).

28. Wright, K.M. & Oparka, K.J. The fluorescent probe HTPS as a phloem-mobile, symplastic tracer: an evaluation using confocal laser scanning microscopy. *J. Exp. Bot.* **47**, 439–445 (1996).

Supplementary Table 2. Fluorophores tested in this study. Molecular masses and charges at pH 7 based on the suppliers' information (which sometimes is incomplete) and the PubChem database of the National Institutes of Health, USA (https://pubchem.ncbi.nlm.nih.gov/) are shown with the number of independent biological replicates in this study for each fluorophore.

Fluorophore	Mass (Da)	Net Charge (at pH 7)	Supplier	Biological Replicates
Acridine Yellow	237	+2	Thermo Scientific	5
Safranin O	315	+2	Sigma Aldrich	6
Fluorescein (Uranin)	332	−2	Sigma Aldrich	5
MitoTracker Orange	392	+1	Invitrogen (Molecular Probes)	5
Rhodamine B	443	0	Sigma Aldrich	6
Rhodamine 6G	443	+1	Sigma Aldrich	8
Lucifer Yellow CH	443	−2	Sigma Aldrich	7
HPTS	455	−3	Sigma Aldrich	13
Cyanine 5 hydrazide	499	+1	Kerafast	13
ATTO Thio12	502	0	ATTO-Tec	6
ATTO 565	512	−1	ATTO-Tec	11
Alexa Fluor 488 hydrazide	547	−2	Invitrogen (Thermo Fisher Scientific)	27
Sulforhodamine B	559	−1	Biotium	5
Sulforhodamine 101	607	−1	MedChemExpress	5
ATTO 647N	642	0	ATTO-Tec	5
ATTO 532	646	−2	ATTO-Tec	5
Alexa Fluor 568 cadaverine	777	−1	Molecular Probes (Life Technologies)	9
CF 488A hydrazide	~ 928	−1	Sigma Aldrich	6
Alexa Fluor 633 hydrazide	~1027	−2	Invitrogen (Thermo Fisher Scientific)	12

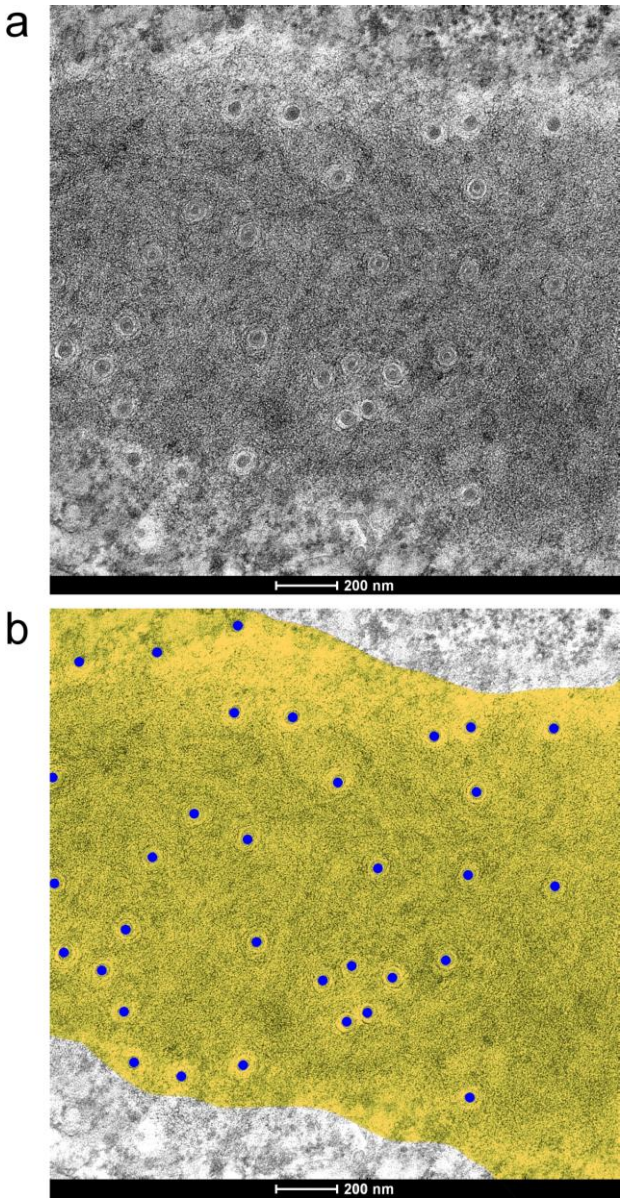

Supplementary Figure 1. Determination of plasmodesma density in cell walls of *Tradescantia* stamen hair cells. a, Section of a cell wall at a shallow angle showing numerous plasmodesmata (compare Fig. 1e). The total area covered by the micrograph is 3.47 μm^2. **b**, The exact location of the border between cell wall and cytoplasm is not sharply discernible on such sections and has to be estimated. The wall is marked by a yellow overlay in this image, and 33 visible plasmodesmata are highlighted by blue dots. With an estimated wall area of 2.93 μm^2, plasmodesma density is 11.3 μm^{-2} in this image.

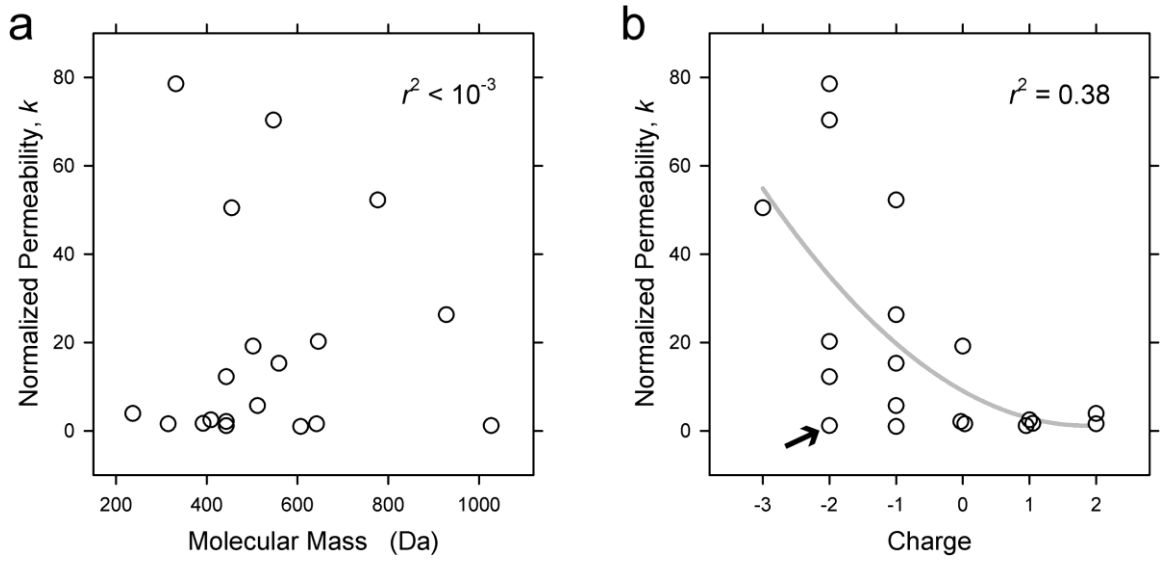

Supplementary Figure 2. Dependence of plasmodesmal permeability *k* on molecular mass (a) and electric charge (b) of the 19 fluorophores tested. Data shown represent the medians of the biological replicates of each fluorophore; these medians were normalized to the smallest observed value. Coefficients of determination (r^2) are indicated in **a** and **b**. The grey line in **b** is a second order polynomial fitted to visualize the general trend towards greater permeabilities for anionic fluorophores. The datapoint highlighted by an arrow in **b** represents Alexa Fluor 633, the largest fluorophor tested. If we assume that this large molecule is geometrically excluded and omit it from analysis, r^2 will rise to 0.48.

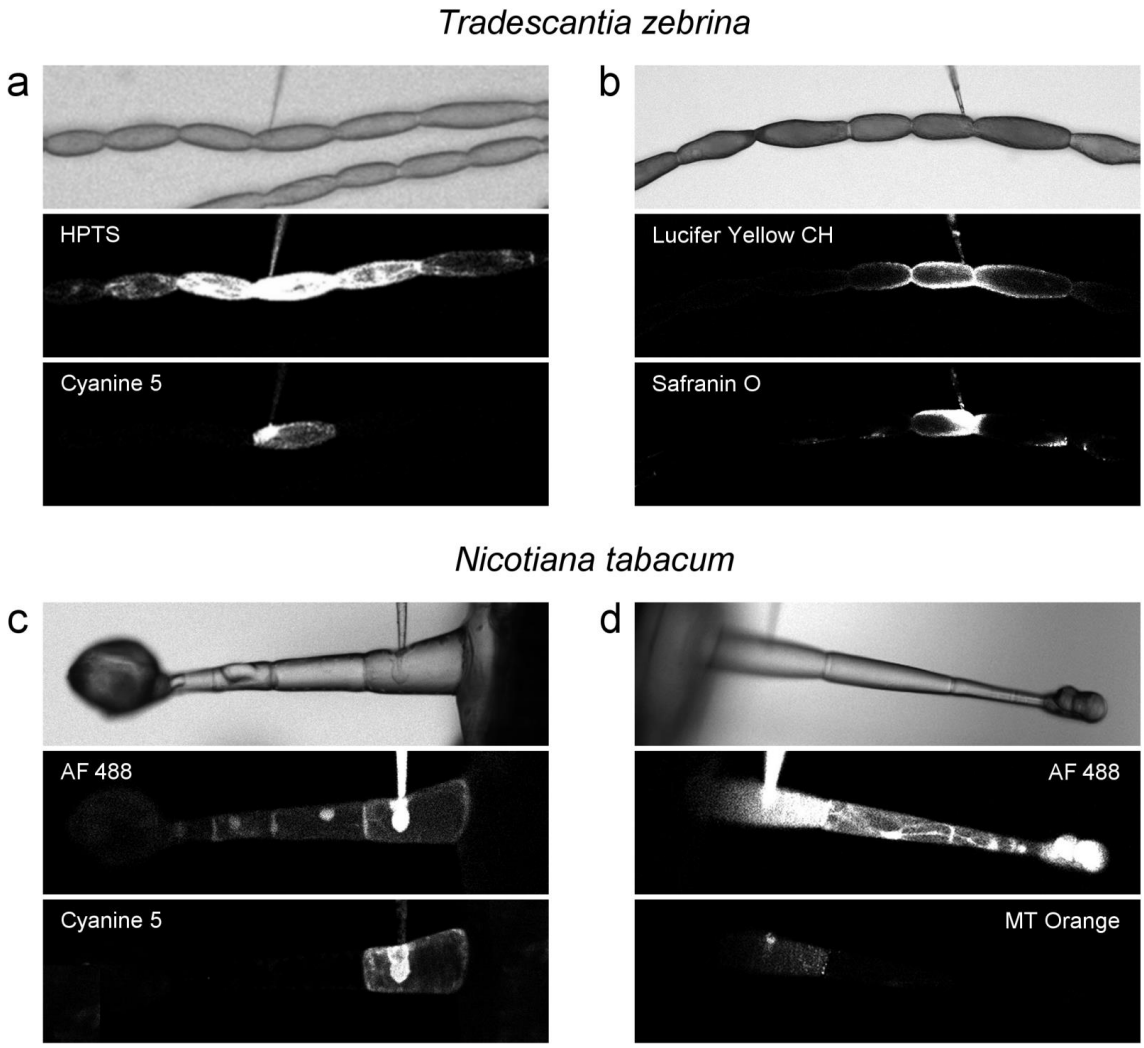

Supplementary Figure 3. Cell-to-cell movement of anionic but not cationic fluorophores in *Tradescantia* stamen hairs and *Nicotiana* trichomes. Combinations of one of the anionic fluorophores HPTS (**a**), Lucifer Yellow CH (**b**), and Alexa Fluor 488 (**c**, **d**) with one of the cationic fluorophores Cyanine 5 (**a**, **c**), Safranin O (**b**), and MitoTracker Orange (**d**) were injected with DIMPs into a cell in the centre of a *Tradescantia* stamen hair (**a**, **b**) or the basal cell of a *Nicotiana* epidermal trichome (**c**, **d**). After 12 minutes, all fluorophores were detectable in the injected cell, but only the anionic ones had moved into adjacent cells. Width of the micrographs: **a**, **b**, 800 µm; **c**, **d**, 450 µm.

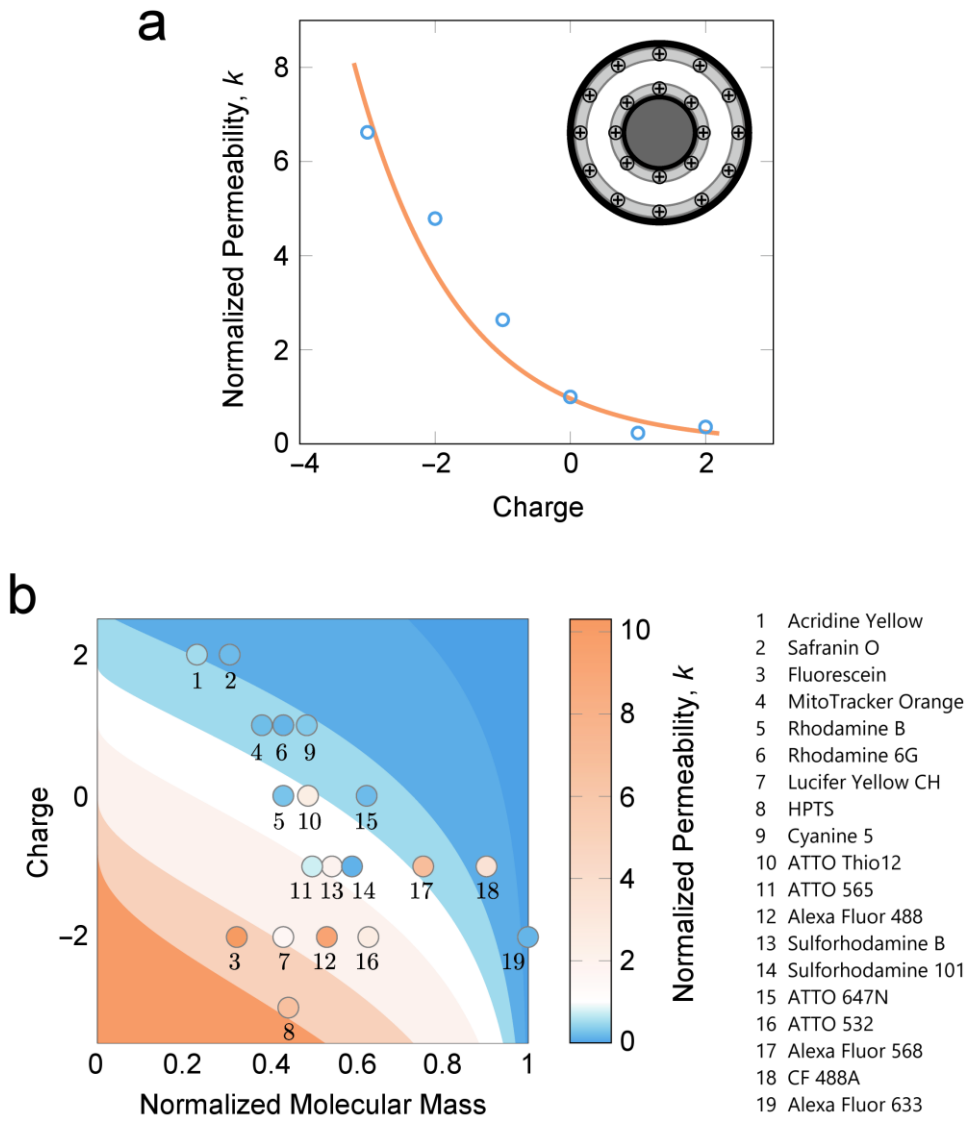

Supplementary Figure 4. Comparison of experimentally observed plasmodesmal permeabilities, *k*, with theory. a, Plot of fluorophore permeabilities normalised by the average permeability of the neutral fluorophores (circles) as a function of charge; values are the means of the medians of the biological replicates for each charge. The line shows a fit of the normalised theoretical permeability as a function of charge (Eqs. (3) and (5) in Ref. 1) with the surface potential ζ as the only fitting parameter. The surface potential is found as ζ = 40 mV. The theory in Ref. 1 was modified to include the particle size by changing the limits of the integral in the diffusion cross-section in Eq. (3) to the area available to the centre of a spherical particle of radius *s*. The theory is normalised by the neutral case, with the particle size found using the

mean molecular weight of the neutral fluorophores. The sizes of the fluorophores are estimated from their molecular weight, assuming the largest fluorophore has a diameter equal to the cytoplasmic sleeve width h. We used h = 3 nm and the thickness of the electrical double layer λ_D = 1 nm (corresponding to a bulk electrolyte concentration of approximately 100 mM at room temperature; Ref. 2). The concentric geometry is approximated by a parallel plate geometry as the gap between the pore wall and the desmotubule is much smaller than the radii of either. We have simplified the surface charge distribution as shown in **a** and assume the surface potential is the same on both surfaces. The theory is valid when the concentration of the diffusing fluorophores is much smaller than the concentration of ions in the bulk cytosol, so that the presence of the fluorophores does not affect the size of the electrical double layer. This is the case when the ratio $(c_0 Z^2)\,(c_{el} Z_{el}^2)^{-1} \ll 1$, where c_0 and Z are the concentration at zero surface potential and the valence of the fluorophores, respectively, and c_{el} and Z_{el} are the concentration at zero surface potential and the valence of the ions in the bulk cytosol, respectively (see Ref. 1 for details). Here, the ratio is approximately $(c_0 Z^2)\,(c_{el} Z_{el}^2)^{-1} \approx 0.001$—0.01. **b**, Contour plot of the normalised diffusion cross-section (Eqs. (3) and (5) in Ref. 1, modified to include particle size) as a function of fluorophore charge and normalised molecular mass. The colours of the circles represent the normalised median permeabilities of the 19 fluorophores tested. The same normalisation as in panel **a** is used, along with h = 3 nm, λ_D = 1 nm, and surface potential ζ = 40 mV. The isolines are 10, 5, 2, 1, 0.5, and 0.1.

1. Christensen, A.H., Gupta, A., Chen, G., Peters, W.S., Knoblauch, M., Stone, H.A. & Jensen, K.H. Locally optimal geometry for surface-enhanced diffusion. *Phys. Rev. E* **108**, 045101 (2023).

2. Schoch, R.B., Han, J. & Renaud, P. Transport phenomena in nanofluidics. *Rev. Mod. Phys.* **80**, 839 (2008).